Journal of Electronic Materials (2022) 51:6416–6430
https://doi.org/10.1007/s11664-022-09879-y

ORIGINAL RESEARCH ARTICLE

Polyethyleneimine–Chromium Oxide Nanocomposite Sensor with Patterned Copper Clad as a Substrate for CO_2 Detection

J. R. Naveen Kumar[1,2] · Abdulraheem S. A. Almalki[3] · B. M. Prasanna[4] · P. Prasad[1] · Narayana Hebbar[5] · Abdullah Alsubaie[6]

Received: 26 February 2022 / Accepted: 10 August 2022 / Published online: 4 September 2022

Abstract

Polyethyleneimine (PEI) and chromium oxide (Cr_2O_3) with different weight percentages were chosen for sensing carbon dioxide (CO_2). Four divergent varieties of sensors with different concentrations of Cr_2O_3 in PEI were fabricated by drop-casting the sensitive films on prepared interdigitated electrodes (IDE) from copper clad. X-ray, absorbance, morphological, and compositional studies were carried on Cr_2O_3 nanoparticles by x-ray diffractometry (XRD), UV–Visible spectrometry, and field-emission scanning electron microscopy (FESEM). Response proficiency for all the fabricated sensors was meticulously examined at room temperature. Solitary proficiencies of resistance versus gas concentration, sensitivity, repeatability, and precise response time and recovery time measurements were examined. It was epitomized that the appropriate weight ratio of PEI and Cr_2O_3 was critical for CO_2 sensing. A reasonable correlation between the sensing responses of the developed sensors to carbon dioxide under nitrogen was achieved.

Keywords Chromium oxide · carbon dioxide · copper clad · IDE

Introduction

Sensors are devices or a subsystem that detect changes in the surrounding environment, and send the collected data to the remaining electronic blocks for processing.[1–3] Sensors are used in several day-to-day devices, such as light sensors, which help with the auto-brightness function for the display. This is an essential function, because the light sensor detects the light levels of the environment in which the user is using the device and can adjust the brightness automatically. Most people are unaware of its countless applications.[4–6] Applications of sensors can be seen in automotives, aircraft, machinery, manufacturing, and various other sectors of everyday life. A wide variety of sensors measures material physical and chemical characteristics. Some of the examples include vibrational sensors, electrochemical sensors, gas sensors, and fluid viscosity measurement sensors.[7–10]

Gas detectors or sensors are electronic gadgets that sense and recognize various categories of gases. Primarily, they are used to identify and measure the gas concentration of explosive or toxic gases.[11–13] These types of sensors are used in manufacturing industries to detect gas leakages and smoke, and in homes to monitor the concentration of carbon monoxide or carbon dioxide. Gas sensors vary in their ability to sense and detect range and size. Gas sensors have to be calibrated more frequently than other kinds of sensors, as they are in frequent contact with atmospheric air and other kinds of gases.[14–16] Gas sensors detect the metal oxide change in electrical resistance when interacting with target gases. Gas sensors have a wide range of applications in forecasting and avoiding many possible hazards, and

✉ B. M. Prasanna
drbmprasanna@gmail.com

1 Department of Nano Technology, Srinivas Institute of Technology, Valachil, Mangaluru, India

2 Department of AIML, Institute of Engineering and Technology, Srinivas University, Mangaluru, India

3 Department of Chemistry, Faculty of Science, Taif University, Taif 21974, Saudi Arabia

4 Department of Chemistry, Bapuji Institute of Engineering and Technology, (Affiliate to Visveswaraya Technological University, Belagavi), Davanagere, Belagavi 577 004, India

5 Department of Chemistry, Sri Dharmasthala Manjunatheshwara College (Autonomous), Ujire 574 240, India

6 Department of Physics, College of Khurma, Taif University, P.O. Box 11099, Taif 21944, Saudi Arabia

must conform to safety standards in industrial and domestic environments. They need to be located precisely to detect the level of accumulation of any gas before it becomes hazardous.[17,18] The spatial and temporal distribution of CO_2 at the earth–atmosphere interface, and at the boundary layer above it, is of great importance for soil, agricultural, and atmospheric sciences. In general, root respiration and soil microbial activity are the main sources of high CO_2 concentrations at this border layer. Enhanced detection of CO_2 gas concentration could lead to a better understanding of agricultural productivity and transport mechanisms at this crucial interface.[19–22] Accurate monitoring of CO_2 can improve modeling and decision-making to enhance agricultural productivity, thus allowing farmers to meet rising food demands, while also making their lives more accessible.[23] Using a gas sensor to detect CO_2 concentration in the atmosphere inside a structure is a cost-effective way of maintaining adequate air circulation for our comfort and avoiding over-ventilation, which can increase heating and cooling expenses.[24–26] Thin films play a vital role in sensing and other applications.[27,28] Polyethyleneimine (PEI), reduced graphene oxide, and cerium oxide can be used as potential materials for CO_2 sensing at room temperature.[29,30] The nano-architectonics concept is supposed to involve the architecting of functional materials using nanoscale units based on the principles of nanotechnology.[31] A graphene and metal oxide combination has also shown effectiveness in gas sensing.[32] This work mainly focuses on the potentiality of the PEI–Cr_2O_3 nanocomposite for carbon dioxide sensing with varying percentages.

Experimental

Precipitation Method for Chromium Oxide Synthesis

Chromium sulfate was used as a precursor material or prospective source of chromium, while ammonium hydroxide was used as a precipitating reagent in the production of chromium oxide (Cr_2O_3). Figure 1 shows a schematic of Cr_2O_3 synthesis, which typically involves five steps,

Step 1. 250 mL of 0.1 M chromium sulfate solution were dissolved in distilled water and aqueous ammonia was prepared.

Step 2. Liquid aqueous ammonia was added dropwise until the pH of the reaction mixture reached 10 under continuous stirring on a magnetic stirrer. When the pH came close to 10, precipitation of the reaction mixture started, and was a maximum at 10.

Step 3. The obtained precipitation was collected and filtered by vacuum filtration and washed with distilled water.

Step 4. The filtered residue was dried in a hot air oven for 24 h at 80°C.

Step 5. The obtained mass was crushed using pestle and mortar to obtain Cr_2O_3 powder.

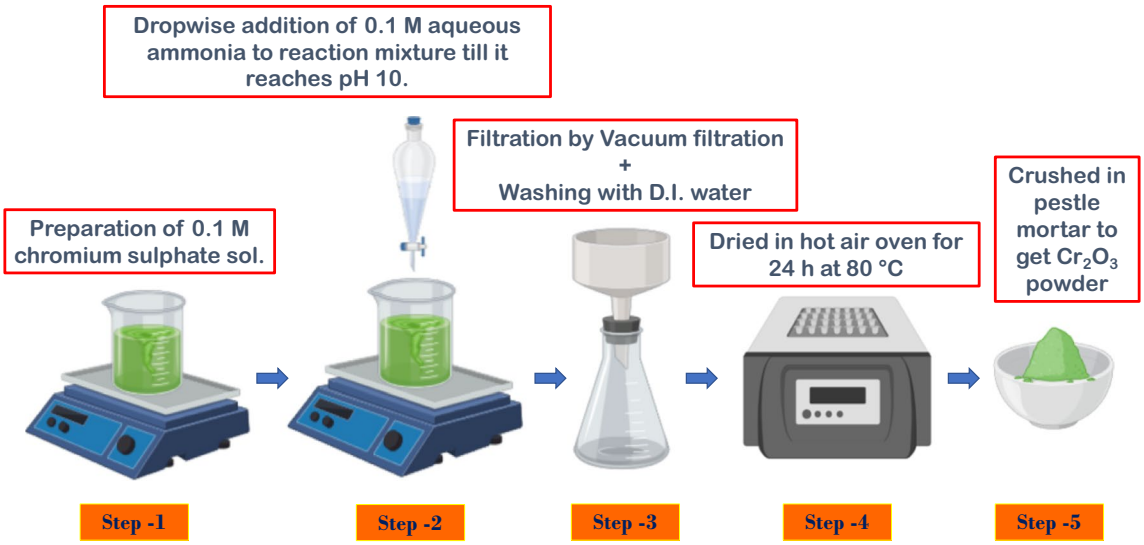

Fig. 1 Schematic of the synthesis of chromium oxide.

Experimental

Interdigitated Electrode (IDE) Preparation by Copper Clad for PEI–Cr_2O_3 Nanocomposite Sensor

Copper clad, permanent markers, ferric chloride powder, a cutter, and a glass Petri dish were required to prepare the interdigitated electrodes (IDE) by copper clad. For the IDE substrates, copper clad is used as the base material. Ferric chloride powder acts as an etching agent, and permanent markers were used as the etch resistant while pattering the copper clad to form the IDE. Figure 2 depicts the process of preparing and coating of the IDE from the copper clad, consisting of four steps,

Step 1. The copper-clad (Tech Delivers) was carefully cut into four pieces with the dimensions of 2 cm × 1 cm.
Step 2. The IDE pattern was uniquely marked onto the four pieces of copper clads with the help of a permanent marker.
Step 3. The patterned copper clads were selectively etched for 15 min in ferrous chloride solution (etching solution).
Step 4. The patterned copper clads were removed from the etching solution and gently washed with diluted acetone in order to remove the pattern drawn with a marker. IDEs were produced after several washes with distilled water.

PEI–Cr_2O_3 Nanocomposite Sensor Fabrication

PEI was combined with varying concentrations of 0.25 wt.%, 0.50 wt.%, 0.75 wt.%, and 1.00 wt.% of Cr_2O_3 for four different sensors to develop a sensitive layer for the precise detection of CO_2. The coating of the sensitive layer on the IDE is shown in Fig. 3. The following steps are involved,

Step 1. *Stirring* Initially, 2 wt.% PEI was dissolved in distilled water at 50°C, and, once the PEI was entirely dissolved, the polymer was ready for the next step.
Step 2. *Homogenizing* 0.25 wt.%, 0.50 wt.%, 0.75 wt.%, and 1.00 wt.% Cr_2O_3 were added to four test tubes (blending tubes), each containing 25 mL of PEI polymer solution, and the mixture was well combined with a homogenizer to achieve a homogeneous solution.
Step 3. *Drop-casting* With the help of a micropipette, a homogeneous solution of PEI–Cr_2O_3 was drop-cast onto the prepared IDE.
Step 4. After allowing adequate time for the droplets to spread properly, the drop-cast film on the IDE was dried in a hot air oven.

Figure 4 shows the functional components in the PEI–Cr_2O_3 nanocomposite sensor, which contains the four main elements of the sensitive layer of PEI–Cr_2O_3 to detect CO_2, a substrate, an electrode that serves to supply electric potential, and wires for connecting the sensors to the devices.

PEI–Cr_2O_3 nanocomposite sensor setup and measuring of CO_2Gas

Figure 5 shows an instrumental setup used for testing the PEI–Cr_2O_3 nanocomposite sensor. Primarily, two major gases were used in the study:

1. Carbon dioxide (CO_2) gas served as the target gas

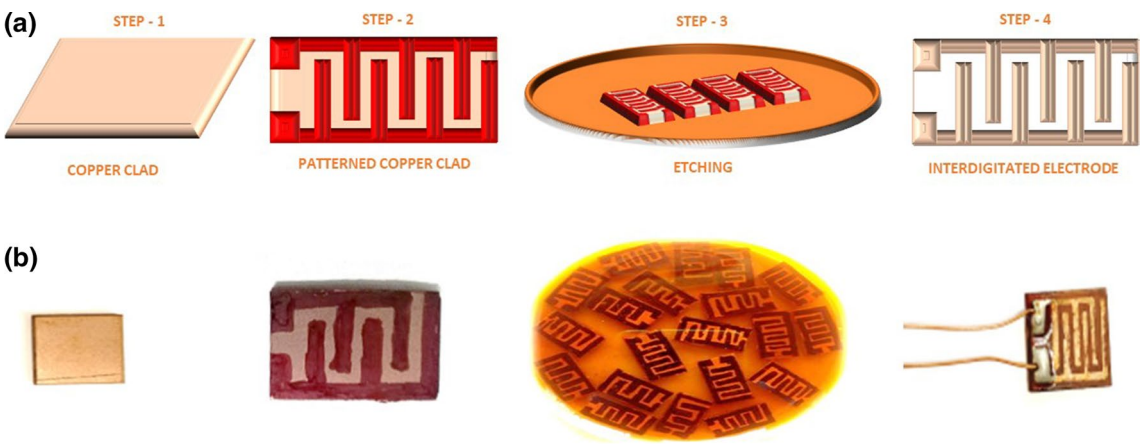

Fig. 2 (a) Schematic of preparing IDE from copper clad, (b) images of preparing IDE from copper clad.

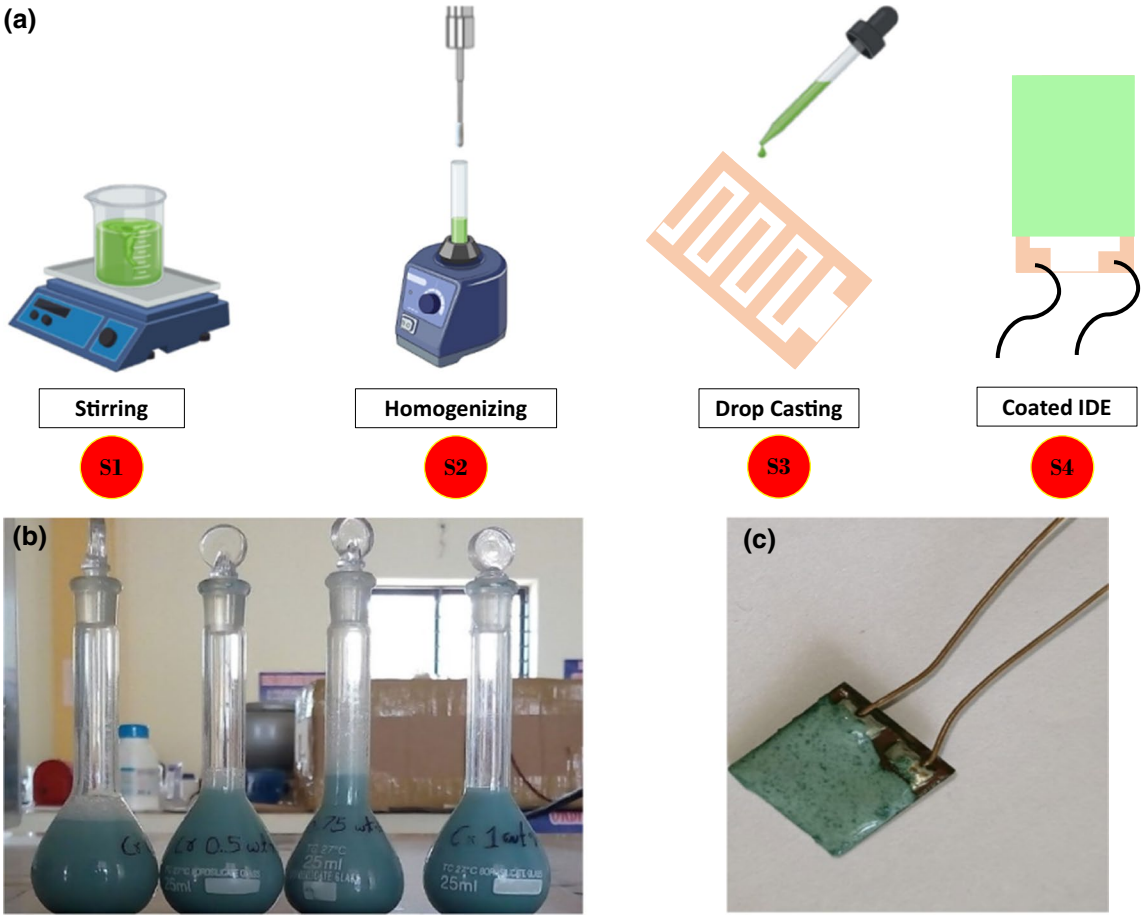

Fig. 3 (a) Schematic of the preparation of a sensitive layer (PEI–Cr_2O_3) and coating on the IDE, (b) image of homogenized PEI–Cr_2O_3 nanocomposite, (c) image of PEI–Cr_2O_3-coated sensor.

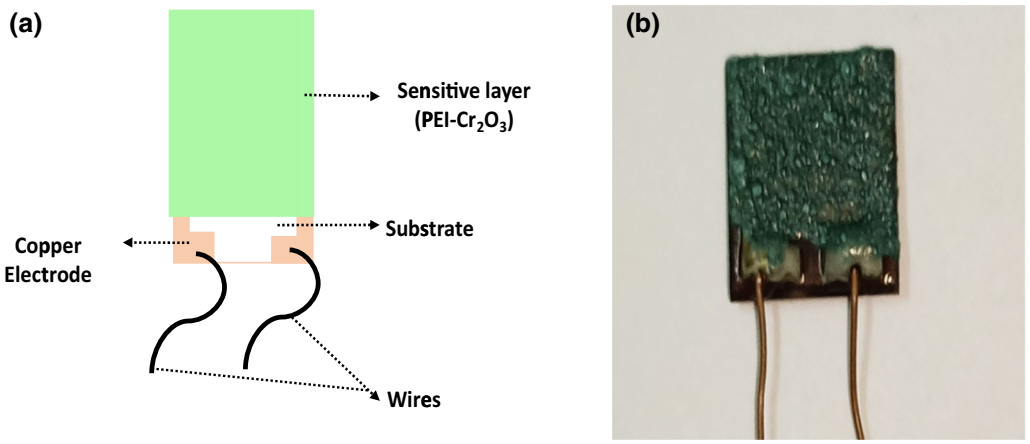

Fig. 4 (a) Schematic of fabricated CO_2 sensor (PEI–Cr_2O_3), (b) image of the sensor.

2. Nitrogen (N_2) gas was used as the carrier, purge, and dilution gas instead of air, to avoid the probable effect of moisture and oxygen present in the air.

The results were examined at room temperature in an atmosphere of nitrogen gas. A mass flow controller was used to accurately control the concentration of CO_2 and N_2 .

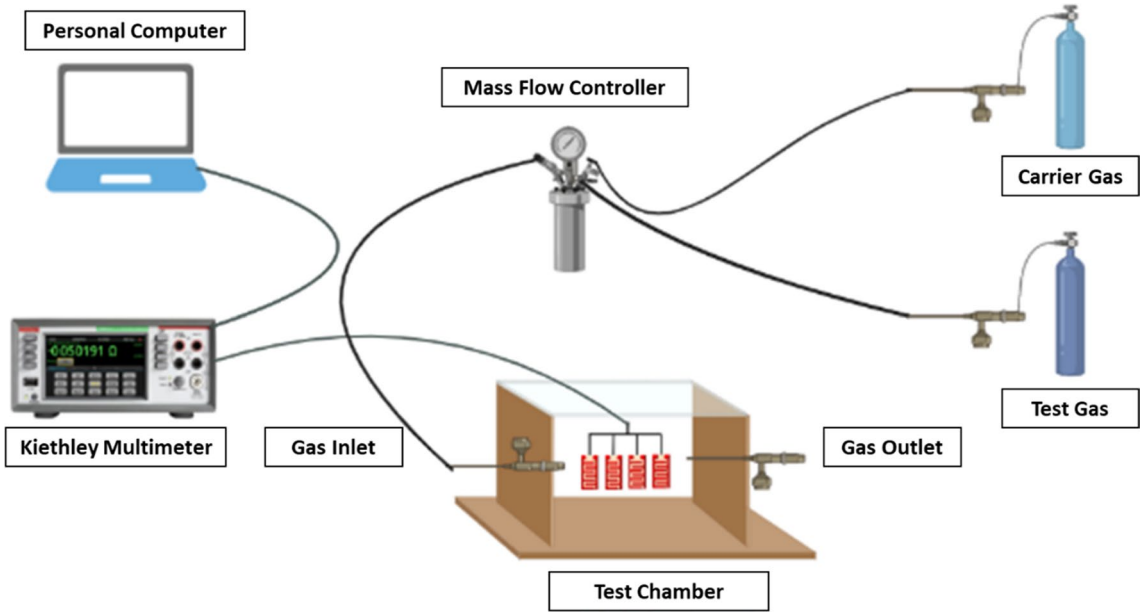

Fig. 5 Schematic of the instrumental setup.

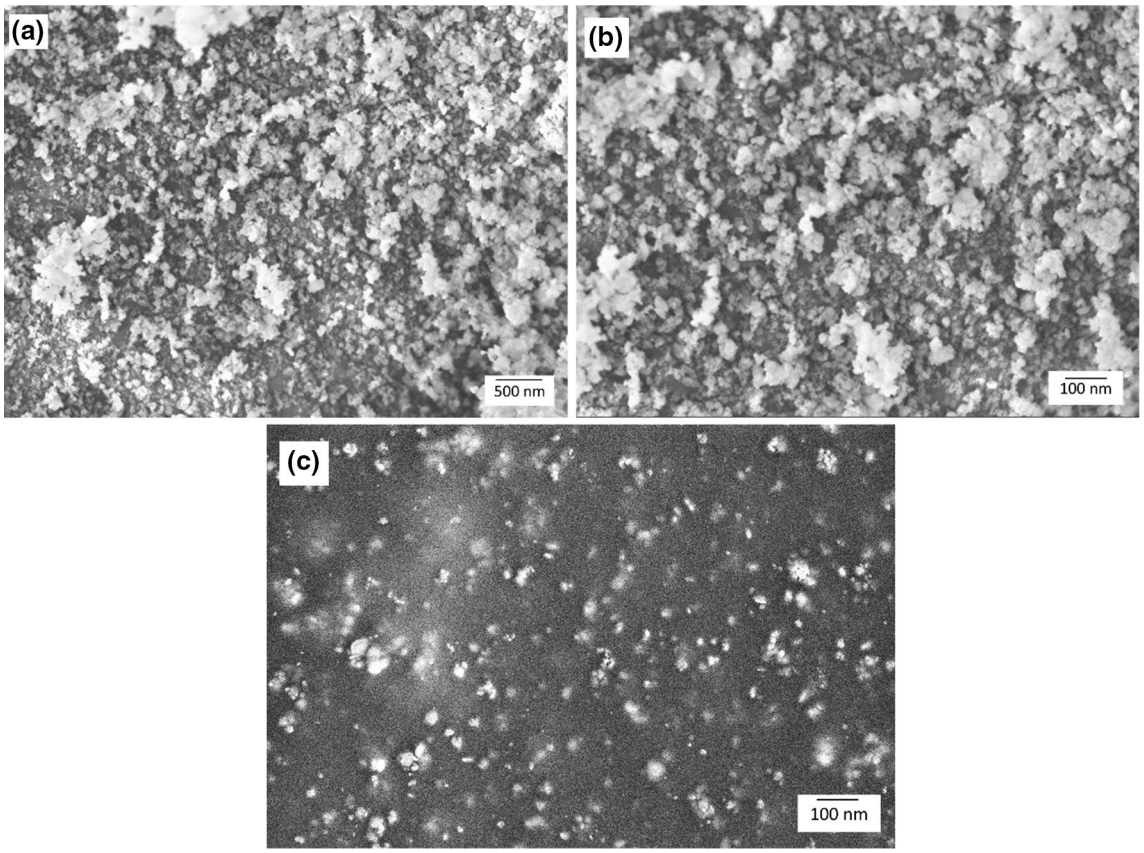

Fig. 6 FESEM images of (a) Cr_2O_3 nanoparticles at 500-nm scale, (b) Cr_2O_3 nanoparticles at 100-nm scale, and (c) PEI–Cr_2O_3 nanocomposite at 100-nm scale.

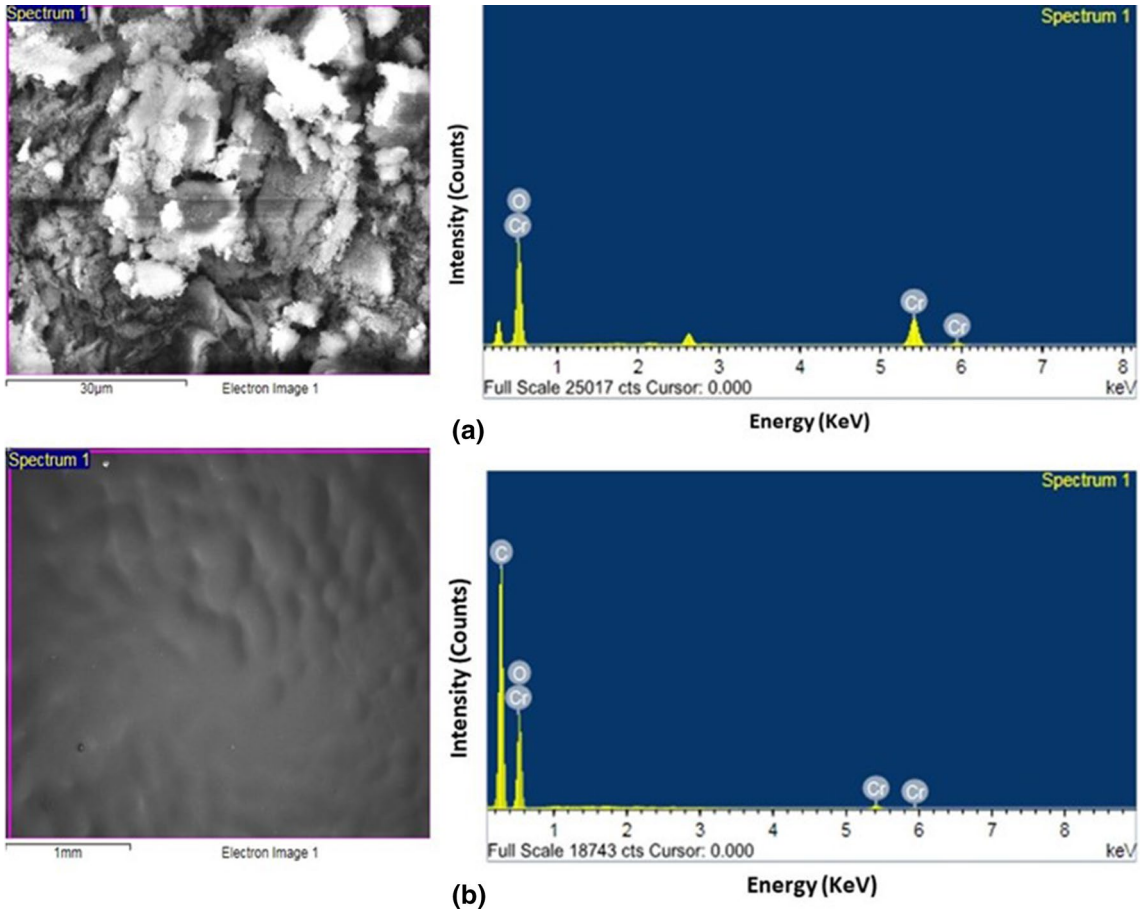

Fig. 7 EDX analysis of (a) Cr_2O_3 nanoparticles (b) PEI–Cr_2O_3 nanocomposite.

Table I Elemental composition of Cr_2O_3 nanoparticles

Element	Weight%	Atomic%
O K	46.95	57.73
Cr K	53.05	42.27
Total	100	

Table II Elemental composition of PEI–Cr_2O_3 nanocomposite

Element	Weight%	Atomic%
O K	67.52	65.25
Cr K	11.54	4.70
C	20.94	30.05
Total	100	

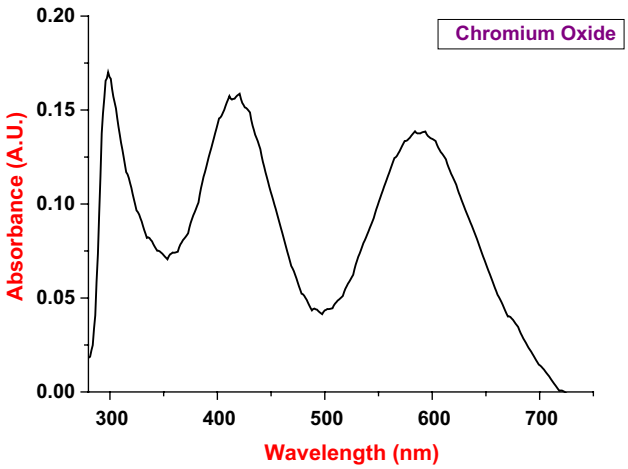

Fig. 8 UV–visible spectra of synthesized Cr_2O_3.

The sensors were kept inside a sealed chamber while nitrogen gas was passed through to mitigate the effect of humidity on the capability of the sensors. Also, the gas inflow rate was kept constant at 300 mL/min so that a strong reference line could be obtained quickly. The electric resistances of the four separate sensors against CO_2 were determined by a Keithley 2700 model multimeter (Keithley Instrument). A personal computer collected the data or equivalent information with appropriate hardware and software. The following are some of the steps taken to evaluate the sensors' performance.

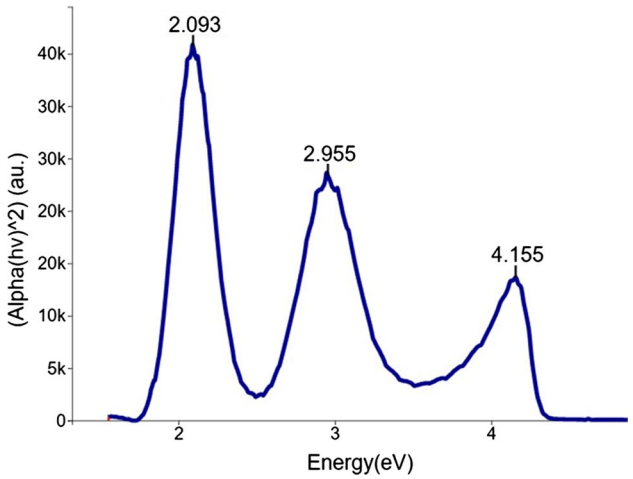

Fig. 9 Tauc plot of Cr_2O_3.

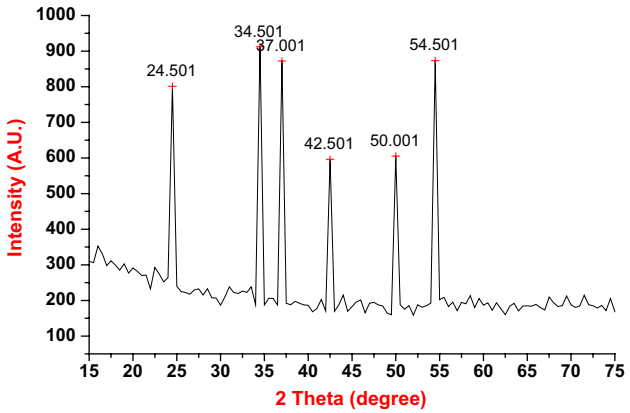

Fig. 10 XRD pattern of Cr_2O_3.

Table III Interplanar distance analysis results of Cr_2O_3

Peak	2-Theta	Theta	Theta in radians	d-Spacing (nm)
1	24.501	12.2505	0.21381156	0.363312977
2	34.501	17.2505	0.301078023	0.259956242
3	37.001	18.5005	0.322894638	0.242946291
4	42.501	21.2505	0.370891193	0.212693652
5	50.001	25.0005	0.43634104	0.182407066
6	54.501	27.2505	0.475610948	0.168362275

Step 1. CO_2 and N_2 were considered as the target and carrier gases.

Step 2. The gas concentration was precisely controlled by a mass flow controller.

Step 3. The sensors were kept in a sealed test chamber.

Step 4. N_2Gas was passed to reduce the effect of humidity on the sensors' operational capability. CO_2 gas was also introduced to the test chamber via a gas inlet.

Step 5. The gas inflow rate was kept constant at 300 mL/min to quickly obtain a strong reference line.

Step 6. A Keithley 2700 model multimeter was used to test the electric resistance of the sensors against CO_2

Step 7. Data collection and equivalent information acquisition was by PC.

Characterization

FESEM and EDX Analysis of Cr_2O_3 and PEI–Cr_2O_3

Cr_2O_3 samples were scanned at 30 KX and 50 KX with an electron energy of 5.00 kV. The surface analysis of a Cr_2O_3 and PEI–Cr_2O_3 nanocomposite is shown in Fig. 6, and the morphology of the surface of the Cr_2O_3 appears to be agglomerated with flower-like structures. At the nanometer scale, agglomerated and flower-like structures are visible, and Fig. 6 a and b shows morphological FESEM images at 500- and 100-nm scales. Due to the great purity of the produced Cr_2O_3, energy dispersive x-ray analysis of the Cr_2O_3 reveals only chromium and oxygen in its spectrum. Energy dispersive x-ray investigation of the PEI–Cr_2O_3 nanocomposite revealed the presence of chromium and carbon. The x-ray spectra and composition of the Cr_2O_3 and PEI–Cr_2O_3 nanocomposite analysis are shown in Fig. 7 and Tables I and II, respectively.

UV–Visible Spectrophotometry Analysis of Cr_2O_3

The UV–visible spectra analysis of the synthesized Cr_2O_3 shows strong absorption peaks at 298.4 nm, 420.8 nm, and 584 nm, which are shown in Fig. 8, corresponding to Cr_2O_3. The band gap of the Cr_2O_3 was obtained by the Tauc plot, as shown in Fig. 9. The band gaps obtained from the Tauc plots for the absorption peaks of 298.4 nm, 420.8 nm, and 584 nm are 2.093 eV, 2.955 eV, and 4.155 eV, respectively.

X-ray Diffractometer Analysis of Cr_2O_3

The XRD pattern of Cr_2O_3 is shown in Fig. 10, revealing a crystalline nature and peaks at 24.501, 34.501, 37.001, 42.501, 50.001, and 54.501, ensuring the synthesis of Cr_2O_3. The interplanar distance of cerium oxide was calculated using Eq. 1, and the relevant results of each peak are shown in Table III. The average crystallite size of Cr_2O_3

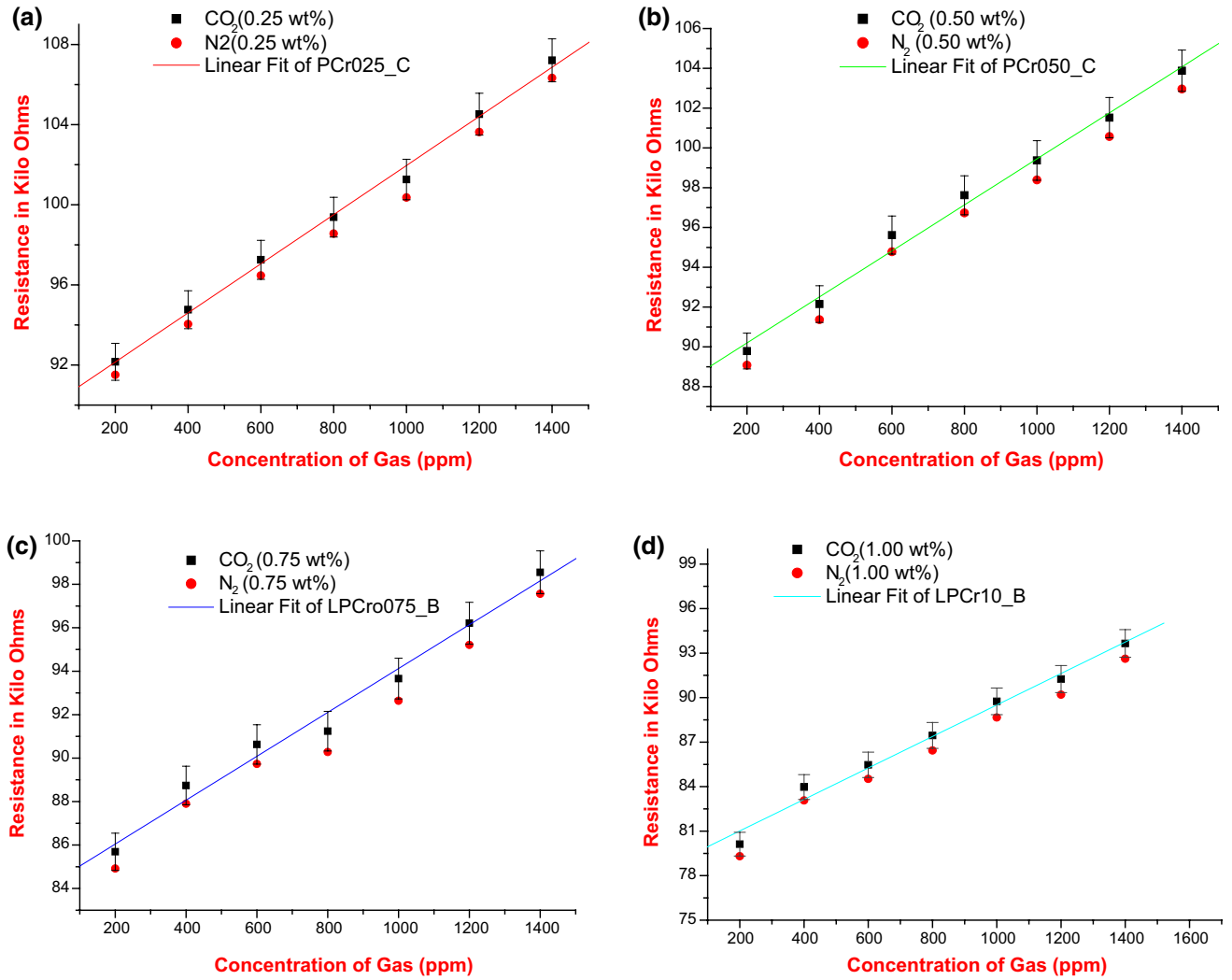

Fig. 11 Resistance versus gas concentration of (a) 0.25 wt.%, (b) 0.50 wt.%, (c) 0.75 wt.%, and (d) 1.00 wt.% of Cr_2O_3 in PEI samples.

Table IV Analysis of resistance against gas concentration results of PEI–Cr_2O_3 nanocomposite sensors

Gas concentration (ppm)	0.25 wt.%		0. 50 wt.%		0.75 wt.%		1.00 wt.%	
	R_g kΩ	R_0 kΩ	R_gkΩ	R_0 kΩ	R_g kΩ	R_0 kΩ	R_g kΩ	R_0 kΩ
200	92.16	91.51	89.79	89.08	85.69	84.92	80.12	79.31
400	94.76	94.04	92.15	91.37	88.74	87.90	83.97	83.07
600	97.25	96.47	95.62	94.78	90.63	89.73	85.47	84.52
800	99.38	98.56	97.62	96.73	91.24	90.28	87.45	86.44
1000	101.26	100.36	99.37	98.39	93.66	92.64	89.75	88.66
1200	104.52	103.63	101.52	100.57	96.21	95.21	91.25	90.20
1400	107.21	106.33	103.88	102.96	98.55	97.56	93.65	92.62

was calculated using Eq. 2 for a maximum peak at 34.501 and Dc = 13.81 nm:

$$d = \frac{n\lambda}{2\sin\theta} \quad (1)$$

where d is the interplanar distance, n the order of reflection ($n = 1$), λ the wavelength of characteristic x-rays (0.15418) and θ the x-ray incidence angle or Bragg's angle (11.1088).

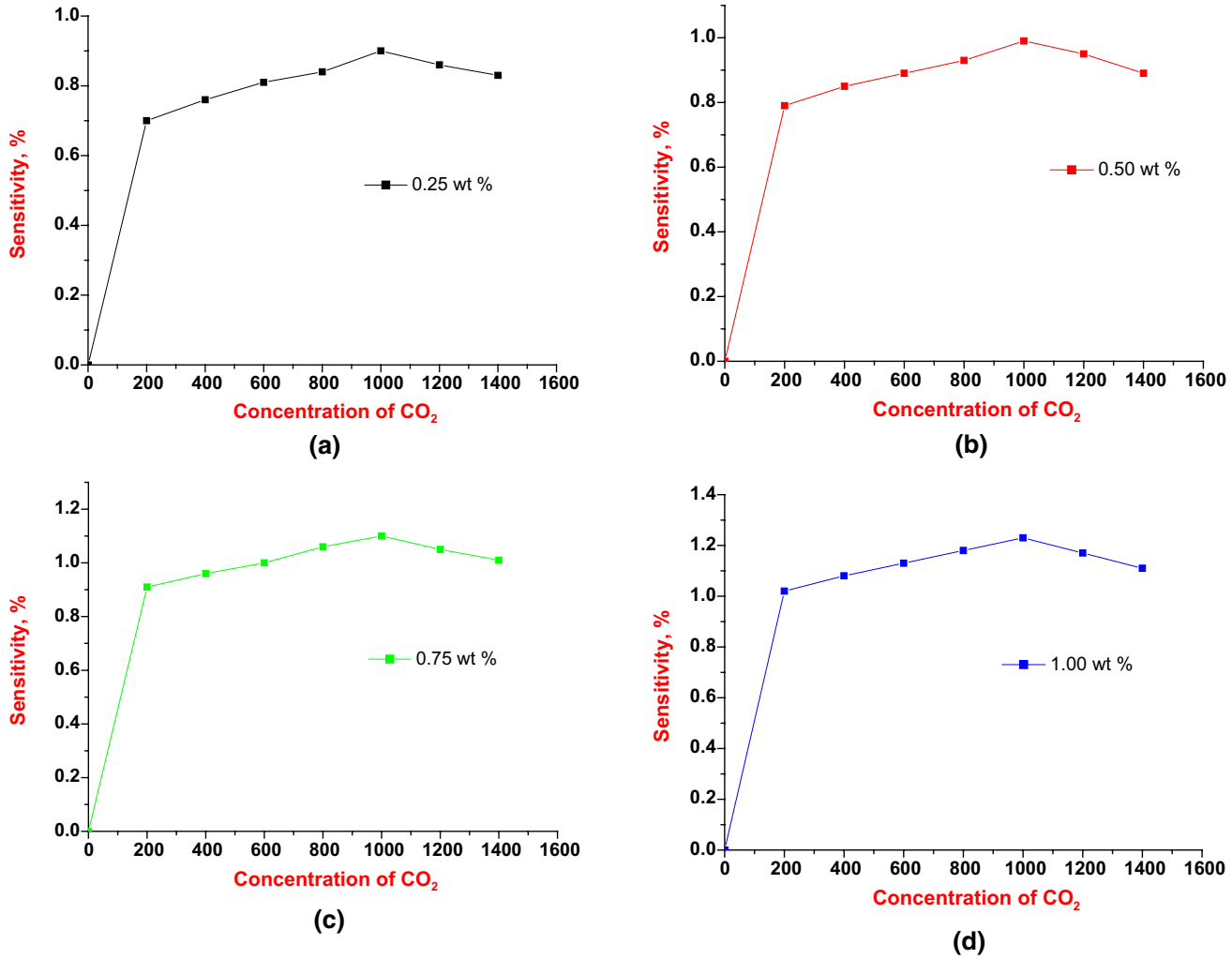

Fig. 12 Sensitivity plots of (a) 0.25 wt.%, (b) 0.50 wt.%, (c) 0.75 wt.%, and (d) 1.00 wt.% of Cr_2O_3 in PEI samples.

Table V Sensitivity analysis results of PEI–Cr_2O_3 nanocomposite sensors

CO_2 concentration (ppm)	Sensitivity of PEI–Cr_2O_3 samples with different wt.%			
	0.25 wt.%	0. 50 wt.%	0.75 wt.%	1.00 wt.%
0	0	0	0	0
200	0.70	0.79	0.91	1.02
400	0.76	0.85	0.96	1.08
600	0.81	0.89	1	1.13
800	0.84	0.93	1.06	1.18
1000	0.90	0.99	1.1	1.23
1200	0.86	0.95	1.05	1.17
1400	0.83	0.89	1.01	1.11

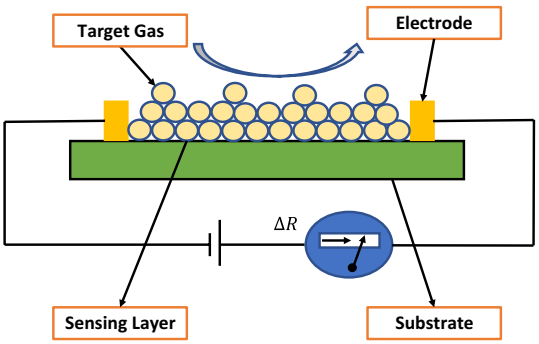

Fig. 13 Sensing mechanism of PEI–Cr_2O_3 nanocomposite CO_2 sensor.

Table VI Sensitivity of the nanocomposites for CO_2 sensors

Sample	Material	Gas concentration (ppm)	Sensitivity%	References	Temperature
1	PEI functionalized PANI film	50–5000	0.00714	33	Room temperature
2	Poly(ionic liquid) nanoparticles	150–2400	0.004	34	
3	1 wt.% of PEI-rGO	1000	1.25	30	
4	1 wt.% of PEI-CeO_2	1000	1.55	29	
5	1wt.% of PEI–Cr_2O_3	1000	1.23	This work	

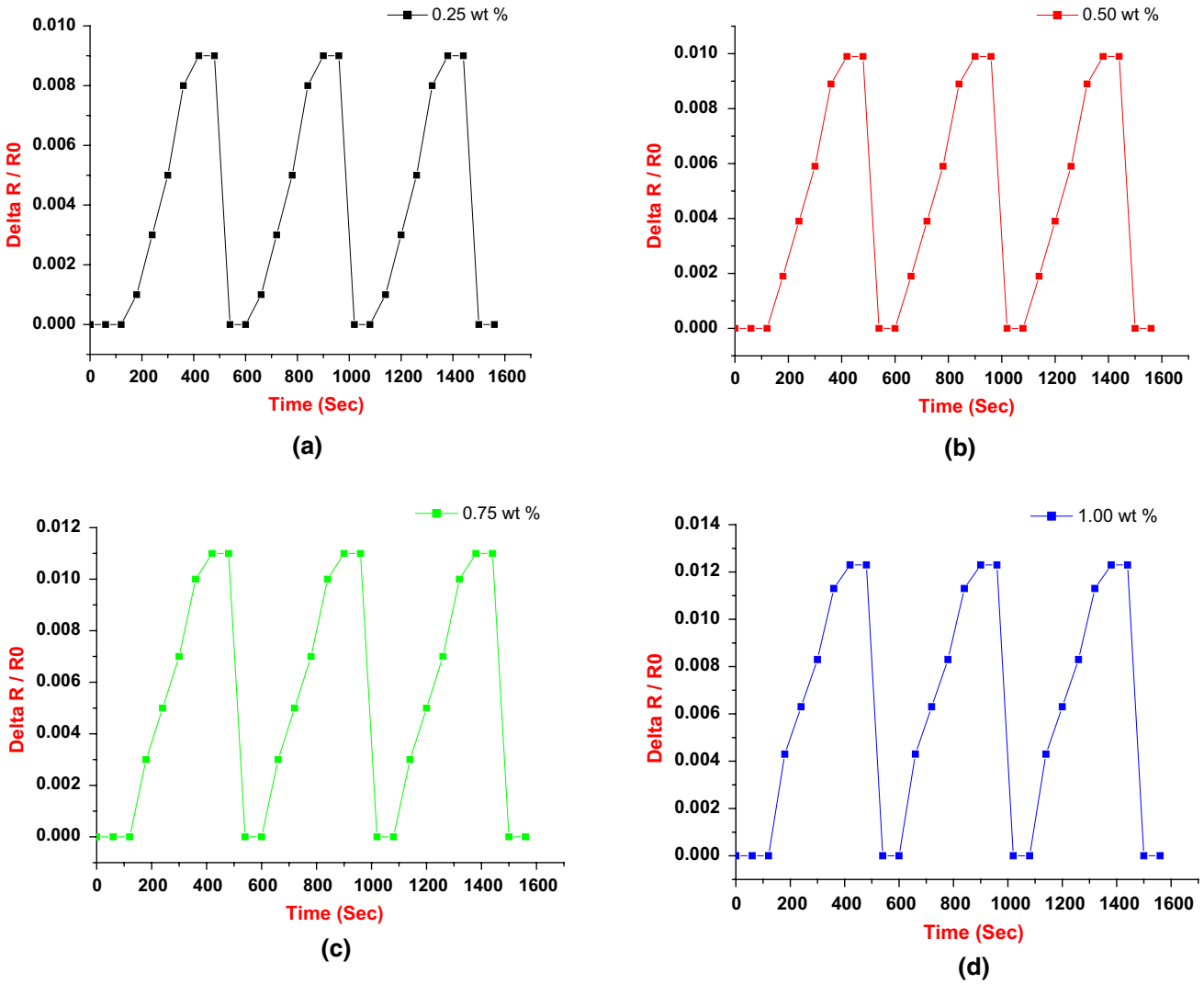

Fig. 14 Repeatability plots of (a) 0.25 wt.%, (b) 0.50 wt.%, (c) 0.75 wt.%, and (d) 1.00 wt.% of Cr_2O_3 in PEI samples.

Table VII Repeatability studies results of PEI–Cr_2O_3 nanocomposite sensors

Time (s)	$\frac{\Delta_R}{R_0}$ of PEI–Cr_2O_3 samples with different wt.%			
	0.25 wt.%	0. 50 wt.%	0.75 wt.%	1.00 wt.%
60	0	0	0	0
120	0	0	0	0
180	0.001	0.0019	0.003	0.0043
240	0.003	0.0039	0.005	0.0063
300	0.005	0.0059	0.007	0.0083
360	0.008	0.0089	0.01	0.0113
420	0.009	0.0099	0.011	0.0123
480	0.009	0.0099	0.011	0.0123
540	0	0	0	0
600	0	0	0	0
660	0.001	0.0019	0.003	0.0043
720	0.003	0.0039	0.005	0.0063
780	0.005	0.0059	0.007	0.0083
840	0.008	0.0089	0.01	0.0113
900	0.009	0.0099	0.011	0.0123
960	0.009	0.0099	0.011	0.0123
1020	0	0	0	0
1080	0	0	0	0
1140	0.001	0.0019	0.003	0.0043
1200	0.003	0.0039	0.005	0.0063
1260	0.005	0.0059	0.007	0.0083
1320	0.008	0.0089	0.01	0.0113
1380	0.009	0.0099	0.011	0.0123
1440	0.009	0.0099	0.011	0.0123
1500	0	0	0	0

$$
\begin{aligned}
Dc &= \frac{0.94\lambda}{\beta \cos\theta} \\
&= \frac{0.94(0.15418)}{(0.01099)\cos(17.2505)} \\
&= \frac{0.1449}{(0.01239)0.95501} \\
&= \frac{0.1449}{0.01049} \\
&= 13.81nm.
\end{aligned} \tag{2}
$$

Results and Discussion

Resistance versus Gas Concentration Studies of PEI–Cr_2O_3 Samples

Resistance versus gas concentration of CO_2 was measured for the PEI–Cr_2O_3 nanocomposite sensors of 0.25, 0.50, 0.75, and 1.00 wt.%. Figure 11 shows that, as the wt.% of PEI–Cr_2O_3 increases, the resistance of the sensor reduces, due to the combination of PEI and Cr_2O_3 and its interaction with CO_2 and N_2 , but the resistance of the sensor increases for the individual wt.% for a varied concentration of CO_2. Resistance versus gas concentration for 0.25 wt.%, 0.50 wt.%, 0.75 wt.%, and 1.00 wt.% PEI–Cr_2O_3 nanocomposite sensors are shown in Table IV. The resistance of 0.25 wt.% PEI–Cr_2O_3 sensors is lower than that of other wt.%.

Sensitivity Analysis of PEI–Cr_2O_3 Samples

Sensitivity is one of the key exposition descriptors for detecting materials to identify CO_2. The sensitivity of PEI–Cr_2O_3 nanocomposite sensors was evaluated using Eq. 3, where the sensor's sensitivity increases with an increase in wt.% of filler material. As seen in Fig. 12, the sensor's sensitivity grew gradually until it reached 1000 ppm CO_2 gas, after which it declined. Table V shows the sensitivity analysis results for 0.25 wt.%, 0.50 wt.%, 0.75 wt.%, and 1.00 wt.% PEI–Cr_2O_3 nanocomposite sensors for different concentrations of CO_2 at the ppm level. The maximum sensitivity% of 1.23 was obtained for the 1.0 wt.% PEI–Cr_2O_3 sample and the minimum (0.90) for the 0.25 wt.% sample. Based on the sensitivity results, the maximum sensitivity was obtained for all wt.% at 1000 ppm of CO_2. As a result, experiments such as repeatability for three cycles, as well as response and recovery times for the entire cycle, were carried out at 1000 ppm CO_2.

$$
Sensitivity = \frac{\Delta R}{R_0} * 100. \tag{3}
$$

The sensing mechanism of the PEI–Cr_2O_3 nanocomposite CO_2 sensor is as shown in Fig. 13, and involves the interaction of amino groups of PEI at room temperature to form carbamates by a reversible reaction, whereas, for Cr_2O_3, it is by physisorption. Desorption was carried out with the aid of nitrogen.

Repeatability Studies of PEI–Cr_2O_3 Samples

PEI–Cr_2O_3 nanocomposite sensors with 0.25 wt.%, 0.50 wt.%, 0.75 wt.%, and 1.00 wt.% repeatability were investigated (Table VI). As illustrated in Fig. 14, PEI–Cr_2O_3 nanocomposite sensors were subjected to 1000 ppm CO_2 for three cycles, each of which took 8 min (4 min for adsorption and 4 min for desorption). Table VII shows the repeatability results of PEI–Cr_2O_3 nanocomposite sensors. The

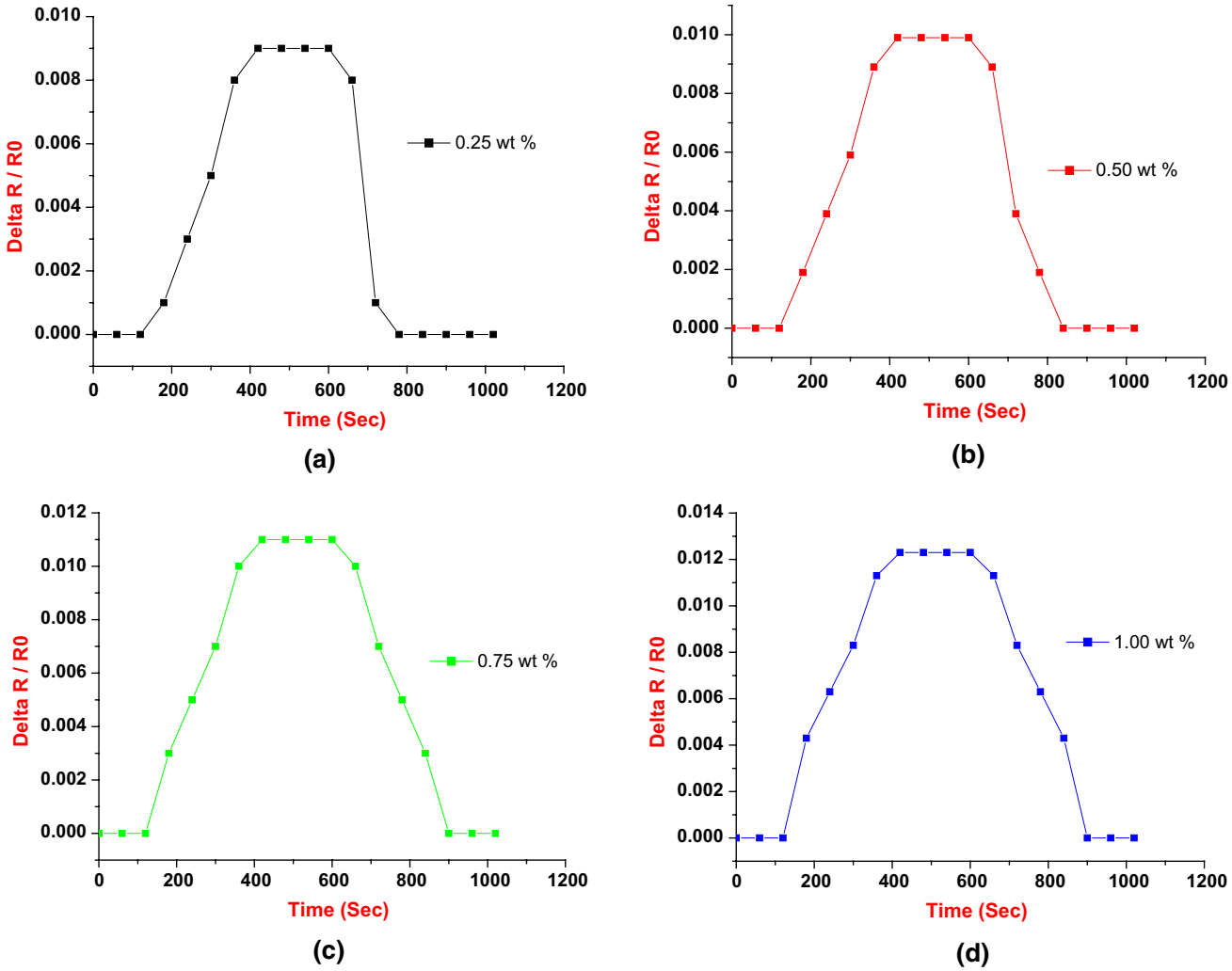

Fig. 15 Response and recovery time plots of (a) 0.25 wt.%, (b) 0.50 wt.%, (c) 0.75 wt.%, and (d) 1.00 wt.% of Cr_2O_3 in PEI samples.

repeatability of 0.25 wt.%, 0.50 wt.%, 0.75 wt.%, and 1.00 wt.% of PEI–Cr_2O_3 nanocomposite sensors were similar. Hence, it can be determined that the repeatability of 1.00 wt.% sensors was better than the others.

Response and Recovery Time Analysis of PEI–Cr_2O_3 Samples

The whole cycle involving adsorption and desorption of PEI–Cr_2O_3 nanocomposite sensors has been examined in terms of response and recovery times. Sensors were exposed to a CO_2 concentration of 1000 ppm until they reached saturation values, followed by desorption with the aid of N_2 until they reached the initial resistance values. It can be seen from Fig. 15 and Table VII that the response time and recovery time of complete cycles of 0.75 wt.% and 1.00 wt.% sensors were about 14 min, which was longer than for the 0.25 wt.% (12 min.) and 0.5 wt.% (13 min) sensors.

Ta and Tb Plots Studies of PEI–Cr_2O_3 Samples

T_a and T_b represent the response time and recovery time of the PEI–Cr_2O_3 nanocomposite sensors, respectively, where the response time is defined as the time taken to reach 9% of equilibrium after the injection of the test gas relevant to changes in the electrical resistance (Table VIII).

The recovery time is defined as the time taken to reach 1% of the electrical resistance when the test gases were removed from the sensor environment. Table IX shows the values of time and Δ_R/R_0 for the PEI–Cr_2O_3 samples sensors with 0.25 wt.%, 0.50 wt.%, 0.75 wt.%, and 1.00 wt.%.

Figure 16 shows T_a and T_b plots of the PEI–Cr_2O_3 nanocomposite with individual wt.%, and a consolidated

Table VIII Analysis of PEI–Cr_2O_3 nanocomposite sensor response and recovery times

Time (s)	$\frac{\Delta_R}{R_0}$ of PEI–Cr_2O_3 samples with different wt.%			
	0.25 wt.%	0. 50 wt.%	0.75 wt.%	1.00 wt.%
0	0	0	0	0
60	0	0	0	0
120	0	0	0	0
180	0.001	0.0019	0.003	0.0043
240	0.003	0.0039	0.005	0.0063
300	0.005	0.0059	0.007	0.0083
360	0.008	0.0089	0.01	0.0113
420	0.009	0.0099	0.011	0.0123
480	0.009	0.0099	0.011	0.0123
540	0.009	0.0099	0.011	0.0123
600	0.009	0.0099	0.011	0.0123
660	0.008	0.0089	0.01	0.0113
720	0.001	0.0039	0.007	0.0083
780	0	0.0019	0.005	0.0063
840	0	0	0.003	0.0043
900	0	0	0	0
960	0	0	0	0
1020	0	0	0	0

plot involving all the results of the 0.25, 0.50, 0.75, and 1.00 wt.% sensors. From Fig. 16 and Table X, it is concluded that the 0.25 wt.% PEI–Cr_2O_3 nanocomposite sensor shows a quick response time of 20 s and a recovery time of 22 s, compared to the other sensors.

Conclusions

In this empirical research, the pertinent materials chosen for the efficient sensing of CO_2 were PEI and Cr_2O_3 used with diverging weight percentages at room temperature. In addition, PEI–Cr_2O_3 nanocomposite film of diverse Cr_2O_3 concentrations was fabricated by drop-casting sensitive films on IDE. The IDEs were created by the copper clad to serve as a substrate. X-ray diffractometry studies showed the crystalline nature and peaks at 24.501, 34.501, 37.001, 42.501, 50.001, and 54.501, which ensures the synthesis of Cr_2O_3. The interplanar distance of the synthesized Cr_2O_3 varied from 0.16 nm to 0.36 nm, and the crystallite size of the maximum at 34.501 is 13.81 nm. The UV–visible spectra analysis of the synthesized Cr_2O_3 shows strong absorption peaks at 298.4 nm, 420.8 nm, and 584 nm. The band gaps obtained from the Tauc plots for the absorption peaks were 2.093 eV, 2.955 eV, and 4.155 eV. FESEM investigation of the agglomerated flower-like shape of the Cr_2O_3 nanoparticles was at 500 and 100 nm dimensions. EDAX spectra of the Cr_2O_3 nanoparticles showed peaks relevant to chromium and oxygen due to the high purity of the Cr_2O_3 nanoparticles. Due to the interaction of PEI and Cr_2O_3 with CO_2 and N_2, the resistance of the sensors reduces as the wt.% of PEI–Cr_2O_3 increases. The sensitivity of the PEI–Cr_2O_3 sensors increased gradually until the CO_2gas of 1000 ppm, and, afterwards, it decreased deliberately, and a maximum sensitivity% of 1.23 was obtained for the 1.0 wt.% PEI–Cr_2O_3 sample. The repeatabilities of the 0.25 wt.%, 0.50 wt.%, 0.75 wt.%, and 1.00 wt.% of PEI–Cr_2O_3 nanocomposite sensors were similar. Hence,

Table IX T_a and T_b analysis results of PEI–Cr_2O_3 nanocomposite sensors

Time (s)	0.25 wt.% sample $\frac{\Delta_R}{R_0}$	Time in s	0.50 wt.% sample $\frac{\Delta_R}{R_0}$	Time in s	0.75 wt.% sample $\frac{\Delta_R}{R_0}$	Time in s	1.00 wt.% sample $\frac{\Delta_R}{R_0}$
0	0	0	0	0	0	0	0
5	0.001	6	0.0019	7	0.003	8	0.0043
10	0.003	12	0.0039	14	0.005	16	0.0063
15	0.005	18	0.0059	21	0.007	24	0.0083
20	0.008	25	0.0089	29	0.01	33	0.0113
26	0.009	30	0.0099	35	0.011	40	0.0123
32	0.009	36	0.0099	42	0.011	48	0.0123
38	0.009	42	0.0099	49	0.011	56	0.0123
44	0.009	48	0.0099	56	0.011	64	0.0123
55	0.008	58	0.0089	66	0.01	74	0.0113
66	0.001	67	0.0039	73	0.007	82	0.0083
75	0	77	0.0019	81	0.005	90	0.0063
–	–	85	0	88	0.003	100	0.0043
–	–	–	–	94	0	106	0
–	–	–	–	101	0	114	0

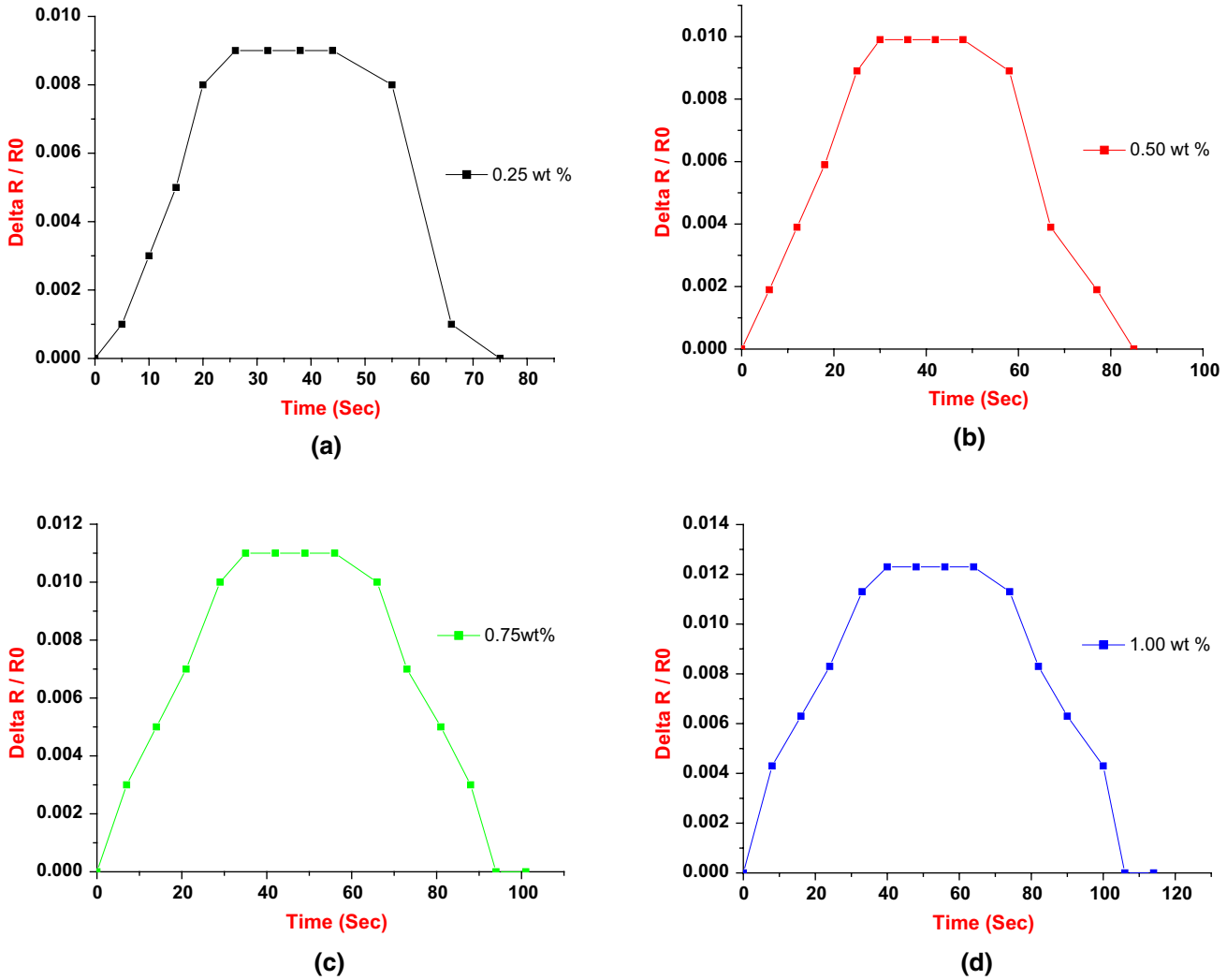

Fig. 16 Ta and Tb plots of (a) 0.25 wt.%, (b) 0.50 wt.%, (c) 0.75 wt.%, and (d) 1.00 wt.% of Cr_2O_3 in PEI samples.

Table X Individual T_a and T_b of PEI–Cr_2O_3 nanocomposite sensors for different wt.%

PEI–Cr_2O_3	0.25 wt.%	0.50 wt.%	0.75 wt.%	1.00 wt.%
T_a	20	25	29	33
T_b	22	29	32	36

it can be determined that the repeatability of the 1.00 wt.% sensor was better than the others. The 0.25 wt.% PEI–Cr_2O_3 nanocomposite sensor shows a quick response time of 20 s and a recovery time of 22 s.

Acknowledgments The authors would like to thank the Ministry of education in Saudi Arabia and Taif University Researchers Supporting Project Number (TURSP-2020/44), Taif University, Saudi Arabia.

Conflict of interest The authors declare that they have no conflict of interest.

References

1. J. Fraden, *Handbook of modern sensors* (New York: Springer, 2010).
2. W.J. Fleming, Overview of Automotive Sensors. *IEEE Sens. J.* 1, 296 (2001).
3. A. Husmann, J.B. Betts, G.S. Boebinger, A. Migliori, T.F. Rosenbaum, and M.L. Saboungi, Mega Gauss Sensors. *Nature* 417, 421 (2002).
4. J. Janata, *Principles of chemical sensors* (Boston: Springer Science and Business Media, 2010).
5. J. Vetelino and A. Reghu, *Introduction to sensors* (Boca Raton: CRC Press, 2017).
6. J.A. Jackman, A.R. Ferhan, and N.J. Cho, Nanoplasmonic Sensors for Biointerfacial Science. *Chem. Soc. Rev.* 46, 3615 (2017).
7. J. Janata, *J. Chem. Sensors. Anal. Chem.* 64, 196 (1992).
8. E. Bakker and M. Telting-Diaz, Electrochemical Sensors. *Anal. Chem.* 74, 2781 (2002).
9. Gustav Gautschi, Piezoelectric sensors, *Piezoelectric Sensorics*. ed. G. Gautschi (Berlin: Springer Berlin Heidelberg, 2002), pp. 73–91. https://doi.org/10.1007/978-3-662-04732-3_5.
10. S. Soloman, Sensors handbook (McGraw-Hill Education, 2010)

11. N. Yamazoe, New Approaches for Improving Semiconductor Gas Sensors. *Sens. Actuators, B Chem.* 5, 7 (1991).
12. G. Sberveglieri, Gas sensors: principles, operation and developments. Springer Science and Business Media (2012)
13. S.R. Morrison, Semiconductor Gas Sensors. *Sensors and Actuators* 2, 329 (1981).
14. C. Wang, L. Yin, L. Zhang, D. Xiang, and R. Gao, Metal Oxide Gas Sensors: Sensitivity And Influencing Factors. *Sensors* 10, 2088 (2010).
15. S.R. Morrison, Selectivity in Semiconductor Gas Sensors. *Sensors and Actuators* 12, 425 (1987).
16. N. Yamazoe, Y. Kurokawa, and T. Seiyama, Effects of Additives On Semiconductor Gas Sensors. *Sensors and Actuators* 4, 283 (1983).
17. J. Åkerberg, M. Gidlund, M. Björkman, Future research challenges in wireless sensor and actuator networks targeting industrial automation. 9th IEEE International Conference on Industrial Informatics, 410 (2011)
18. K. S. Low, W. N. N. Win, M. J. Er, Wireless sensor networks for industrial environments. In International Conference on Computational Intelligence for Modelling, Control and Automation and International Conference on Intelligent Agents, Web Technologies and Internet Commerce (CIMCA-IAWTIC'06) IEEE, 2, 271 (2005)
19. J. Bontsema, E.J. Van Henten, T.H. Gieling, and G.L.A.M. Swinkels, The Effect of Sensor Errors on Production and Energy Consumption in Greenhouse Horticulture. *Comput. Electron. Agric.* 79, 63 (2011).
20. L. Fleming, D. Gibson, S. Song, C. Li, and S. Reid, Reducing N2O Induced Cross-Talk in an NDIR CO_2 Gas Sensor for Breath Analysis Using Multilayer Thin-Film Optical Interference Coatings. *Surf. Coat. Technol.* 336, 9 (2018).
21. D.Y. Kim, A. Kadam, S. Shinde, R.G. Saratale, J. Patra, and G. Ghodake, Recent Developments in Nanotechnology Transforming the Agricultural Sector: A Transition Replete with Opportunities. *J. Sci. Food Agric.* 98, 849 (2018).
22. M. Bhati, K. Bansal, and R. Rai, Capturing Thematic Intervention of Nanotechnology in Agriculture Sector: A Scient Metric Approach. *In Comprehensive Anal. Chem.. Elsevier* 84, 313 (2019).
23. D. Chaudhary, R. Kumar, A. Kumari, R. Jangra, Biosynthesis of Nanoparticles by Microorganisms and Their Significance in Sustainable Agriculture. In Probiotics in Agroecosystem. Springer, Singapore, 93 (2017).
24. R. W. Haines, D. C. Hittle, D. C. Control systems for heating, ventilating, and air conditioning. Springer Science and Business Media. (2006)
25. Y. Xu, Y. Liang, J.R. Urquidi, and J.A. Siegel, Semi-Volatile Organic Compounds in Heating, Ventilation, and Air-Conditioning Filter Dust in Retail Stores. *Indoor Air* 25, 79 (2015).
26. A. Ortiz Perez, B. Bierer, L. Scholz, J. Wöllenstein, and S. Palzer, A Wireless Gas Sensor Network to Monitor Indoor Environmental Quality in Schools. *Sensors* 18, 4345 (2018).
27. K.S. Lokesh, J.N. Kumar, V. Kannantha, and U. Sampreeth, Experimental Evaluation of Substrate and Annealing Conditions on ZnO Thin Films Prepared by Sol-Gel Method. *Mater. Today: Proceed.* 24, 201 (2020).
28. D.S. Mayya, P. Prasad, J.N. Kumar, P. Aswanth, G. Mayur, M. Aakanksha, and N. Bindushree, Nanocrystalline Zinc Oxide Thin Film Gas Sensor for Detection of Hydrochloric Acid, Ethanolamine, and Chloroform. *Int. J. Adv. Res. Sci. Eng* 7, 243 (2018).
29. J.R.N. Kumar, M.B. Savitha, K.S. Lokesh, and H.V. Rohith, CO2 detection: using the polyethyleneimine–cerium oxide nanocomposite sensing film coated on interdigitated electrode prepared from copper clad. *Mater. Res. Innovations* 26, 16–24 (2022).
30. J.R.N. Kumar, Narayana Hebbar, M.B. Savitha, K.S. Lokesh, and Gowda N. Navaneeth, A Potential Application of Polyethyleneimine-Reduced Graphene Oxide Nanocomposite Sensing Film Coated on Interdigitated Electrode Prepared from Copper-Clad for Carbon Dioxide Detection. *Mater. Res. Innovations* 25, 363–371 (2021).
31. K. Ariga, Nanoarchitectonics: What's Coming Next After Nanotechnology? *Nanoscale Horizons* 6, 364 (2021).
32. N. Kumar, M.B. Savitha, and P. Prasad, Graphene-Based Metal Oxide Nanocomposites for Gas Sensing Application. *Int. Journal of Appl. Eng. Manag. Lett. (IJAEML)* 2, 98 (2018).
33. S. Srinivas, T. Sarkar, R. Hernandez, and A. Mulchandani, A Miniature Chemiresistor Sensor for Carbon Dioxide. *Anal. Chim. Acta* 874, 54 (2015).
34. C. Willa, J. Yuan, M. Niederberger, and D. Koziej, When Nanoparticles Meet Poly (Ionic Liquid) S: Chemoresistive CO_2 Sensing at Room Temperature. *Adv. Funct. Mater.* 25, 2537 (2015).